Signal Processing 89 (2009) 87–98

Contents lists available at ScienceDirect

Signal Processing

journal homepage: www.elsevier.com/locate/sigpro

Design of prototype filters for perfect reconstruction DFT filter bank transceivers

François D. Beaulieu *, Benoît Champagne

Department of Electrical and Computer Engineering, McGill University, 3480 University Street, Montréal, Québec, Canada H3A 2A7

ARTICLE INFO

Article history:
Received 25 October 2007
Received in revised form
25 May 2008
Accepted 17 July 2008
Available online 31 July 2008

Keywords:
Multicarrier modulation
DFT filter bank
Perfect reconstruction

ABSTRACT

In recent years, multicarrier modulation techniques have stirred great interest among researchers. One specific form of multicarrier modulation, referred to as orthogonal frequency division multiplexing (OFDM), has been deployed in many applications. Despite their huge popularity, OFDM systems have a few, but important, drawbacks. In particular, OFDM relies on the inverse fast Fourier transform (FFT) for modulation purposes, which leads to a poor spectral containment and, consequently, to a high susceptibility to narrowband noise. To mitigate this problem, we propose to employ over-interpolated perfect reconstruction (PR) discrete Fourier transform (DFT) filter banks. The design of such filter banks is addressed using a novel method that guarantees the PR property to be satisfied while the spectral containment is being maximized. The equalization of frequency-selective channels exploits the fact that the filter banks do not contribute to any distortion due to its PR nature. A simple scheme, taking the form of an one-tap per subcarrier equalizer, is considered. Experimental results indicate that the spectral containment of the proposed PR DFT filter bank transceiver is indeed superior to the OFDM system. Moreover, simulations conducted in a digital subscriber line (DSL)-like environment contaminated by a narrowband noise show that the achievable bit rate of the proposed transceiver is significantly higher than that of a conventional OFDM system.

1. Introduction

Multicarrier modulation (MCM) techniques have been used during the past years in many applications. MCM essentially employs several subcarriers, each of them corresponding to a particular subchannel, to transmit a block of symbols in parallel [1]. These symbols are obtained using standard techniques such as quadrature amplitude modulation (QAM). The constellation size may change from one subcarrier to the other, and this capability can be exploited to either maximize the bit rate or the noise margin [2]. Contrary to frequency-division multiplexing (FDM), the frequency content of adjacent subchannels is allowed to overlap. Even with overlapping frequencies, the transmitted symbols can be recovered perfectly (in noiseless conditions) provided that the block of symbols is modulated using an orthogonal transformation, such as the discrete Fourier transform (DFT).

The DFT or its efficient implementation, the fast Fourier transform (FFT), is the most widely used transform for MCM. For example, it is currently employed in digital subscriber line (DSL) modems [2] and in wireless local area network (LAN) routers [3]. In the literature, DFT-based MCM is commonly referred to by two acronyms, namely, DMT (discrete multitone) or OFDM (orthogonal frequency division multiplexing), depending whether the context is wireline (e.g. DSL technology [2]) or wireless communications [3], respectively. To simplify the terminology, we use in the paper the term "OFDM" regardless of the application.

* Corresponding author. Tel.: +1 514 398 5233; fax: +1 514 398 4470.
E-mail addresses: francois.duplessis-beaulieu@mail.mcgill.ca (F.D. Beaulieu), benoit.champagne@mcgill.ca (B. Champagne).

0165-1684/$ - see front matter © 2008 Elsevier B.V. All rights reserved.
doi:10.1016/j.sigpro.2008.07.014

Despite its popularity, OFDM suffers from a few, but important, drawbacks. Chiefly among them is the considerable overlap between adjacent subchannels, which leads to a very poor spectral containment, and makes OFDM highly sensitive to impairments such as narrowband interference [4]. In DSL, for instance, narrowband noise in the form of radio frequency interference (RFI) arises due to the local loops which can pick up nearby radio transmissions. Amateur radio (or ham) emissions are particularly damaging to OFDM-based DSL modems because of their frequency bands, which overlap those used in DSL, and their high allowable power.

In order to improve the spectral containment of MCM systems and their robustness against narrowband noise, one may consider alternatives to the DFT. Existing solutions include wavelet packet schemes, such as the ones found in [5,6], and offset QAM-based OFDM (OFDM-OQAM) systems [7]. Another very promising option, which has been the focus of many recent publications, is the modulated filter bank-based transceiver [8–25]. In this regard, both the cosine function [8–15], or the complex exponential, via the DFT or the FFT, can be employed [16–25]. In this work, we focus on the DFT filter bank instead of the cosine modulated filter bank. This choice can be explained by the fact that, due to the nature of the cosine transform, only real symbol constellations may be employed. This severely complicates the equalization process, since any phase rotation caused by a non-linear phase channel may not be addressed directly, and the use of computationally expensive post-combiners must then be considered [10]. There exist many approaches for designing DFT filter banks which are appropriate for multicarrier transceivers. Various heuristic methods, using e.g. windowing techniques, are suggested in [22–25]. In [18–21], different techniques are proposed to minimize the intersymbol interference (ISI) caused by the filter bank itself and/or the channel.

The main objective of this paper is to propose a novel method for the design of DFT filter banks suitable for multicarrier transceivers. The aim is to provide better spectral containment to combat impairments such as RFI present in DSL systems. Unlike earlier works (e.g. [16–25]), we design the DFT filter bank using an approach that enforces the perfect reconstruction (PR) criterion. In PR transceivers, equalization is simplified, since one does not need to worry about any distortion generated by the filter bank itself. It might be argued that the performance loss due to a non-PR filter bank is negligible compared to the one introduced by the channel. However, a previous study established that, to properly equalize a non-PR DFT filter bank transceiver, the transmit filters should be equalized using per-subchannel decision-feedback equalizers (DFEs), whereas the channel-induced ISI could solely be mitigated by a one-tap per subcarrier equalizer, provided that the number of subcarriers is high enough [26]. Based on this fact, the computational complexity of a PR DFT filter bank transceiver is greatly reduced compared to a non-PR one since equalization only requires the use of a simple one-tap per subcarrier equalizer instead of expensive per-subcarrier DFEs. Furthermore, computer simulations presented in this paper confirm that the filter-bank-induced distortion present in non-PR filter banks is too severe to be mitigated by a one-tap scheme. Note that the design of the PR filter bank itself is carried out offline, and the computational complexity is the same as the non-PR one if equalization is not taken into account.

The design problem is formulated as an unconstrained minimization problem where the objective is to minimize the stopband energy of the prototype filter. For PR to be theoretically feasible, we consider over-interpolated DFT filter banks, i.e. filter banks where the interpolation factor K is greater than the number of subcarriers M ($K>M$). The minimization process is carried out over a set of real parameters that parametrize the filter coefficients in such a way that PR is automatically achieved. Unlike the similar parametrization-based method proposed in [27], we do not necessarily assume that K is a multiple of M, i.e. $K=2M,3M,\ldots$. The freedom provided by our method in terms of choosing M and K is a key feature that allows the proposed transceiver to have a good bandwidth efficiency. The latter is achieved by keeping the excess bandwidth ratio K/M close to 1, i.e. $K/M\approx 1$.

Results presented in this paper indicate that the spectral containment of the resulting PR DFT filter bank transceiver is much higher than that of an OFDM system. For instance, one particular design with $M=128$ and $K/M=1.25$ is characterized by a stopband energy which is 9 dB lower than the stopband energy of a conventional OFDM system, a notable improvement. Results also show that, under a DSL-like environment, the proposed transceiver outperforms the conventional OFDM transceiver when RFI is present. Indeed, for a 200-m local loop, the achievable bit rate can be improved by a factor of 10 Mbps.

This paper is organized as follows. Background information concerning the PR DFT filter bank transceiver and its polyphase representation is given in Section 2. We present in Section 3 a method to parametrize the prototype filter coefficients such that the resulting filter bank is characterized by the PR property. In Section 4, we explain how this parametrization can be used for the design of a suitable prototype filter. Channel equalization is then discussed in Section 5, where we consider the use of a one-tap per subcarrier equalizer. In Section 6, experimental results are presented. Finally, a conclusion is given in Section 7.

The following notation is used throughout this work. The superscripts T, H and $*$, respectively, stand for the transpose, the Hermitian transpose and the conjugate of a vector or a matrix. All vectors considered in this paper are column vectors, and are denoted by lowercase bold letters, e.g. $\boldsymbol{x}$. We reserve the use of uppercase bold letters for matrices, e.g. $\boldsymbol{A}$. The (i,k) entry of a matrix is represented by $[\boldsymbol{A}]_{i,k}$. The $M\times M$ identity matrix and the $M\times N$ zero matrix are denoted by $\boldsymbol{I}_M$ and $\boldsymbol{0}_{M\times N}$, respectively. Finally, we use the operator $\mathrm{diag}(\boldsymbol{x})$ to represent a diagonal matrix whose diagonal is given by $\boldsymbol{x}$.

2. Proposed transceiver structure

2.1. Time-domain representation

The proposed PR DFT filter bank transceiver is illustrated in Fig. 1. Parameters M and K represent the

number of subcarriers and the upsampling factor, respectively. In this paper, we consider *over-interpolated* filter banks, where $K > M$. Over-interpolation is necessary if we want to satisfy the PR property (see Section 3).

The transceiver operates as follows. M QAM symbols, $x_0[n], \ldots, x_{M-1}[n]$, where n denotes the discrete-time frame index, are obtained from constellation diagrams. For baseband systems such as DSL modems, to ensure that a real signal is sent through the physical channel, these symbols must be conjugate symmetric, i.e. we must have $x_i[n] = x^*_{M-i}[n]$ for $i = M/2+1, \ldots, M-1$, whereas $x_0[n]$ and $x_{M/2}[n]$ must be chosen from a constellation of real symbols. Each symbol $x_i[n]$, $i = 0, \ldots, M-1$, is first expanded by a K-fold expander. The resulting signal, $x^{\mathrm{E}}_i[m]$, where m denotes the discrete-time index at the channel rate, can thus be expressed as

$$x^{\mathrm{E}}_i[m] = \begin{cases} x_i[m/K] & \text{if } m/K \text{ is an integer,} \\ 0 & \text{otherwise.} \end{cases}$$

The expanded signal $x^{\mathrm{E}}_i[m]$ is then filtered by a DFT modulated filter $F_0(zW^i)$, $W \triangleq (1/\sqrt{M})\mathrm{e}^{-\mathrm{j}2\pi/M}$, yielding

$$u_i[m] = F_0(zW^i)x^{\mathrm{E}}_i[m],$$

where z (or z^{-1}) represents the unit advance (or delay) operator, and

$$F_0(z) = \sum_{m=0}^{D-1} f_0[m]z^m$$

is the Z-transform of the so-called prototype filter, a D-tap finite impulse response (FIR) filter with real coefficients $f_0[m]$. Note that for convenience in analysis, $F_0(z)$ is non-causal; in practice, causality can be ensured simply by adding a delay of $D-1$ samples. The expanded and filtered signals $u_i[m]$ are finally added together to form the transmitted signal $u[m]$, i.e. $u[m] = \sum_{i=0}^{M-1} u_i[m]$.

During transmission, the signal is sent through a channel, modelled here by a Q-tap FIR filter $C(z)$ with coefficients $c[m]$, i.e. $C(z) = \sum_{m=0}^{Q-1} c[m]z^{-m}$, and an additive noise $\eta[m]$. The received signal $v[m]$,

$$v[m] = C(z)u[m] + \eta[m]$$

is processed by the receiving filter bank, whose filters are given by $\widetilde{F}_0(zW^0), \ldots, \widetilde{F}_0(zW^{M-1})$. The tilde operator denotes paraconjugation, which is defined as $\widetilde{F}_0(z) \triangleq F^*_0(1/z^*)$ for a scalar function and as $\widetilde{\boldsymbol{G}}(z) \triangleq \boldsymbol{G}^{\mathrm{H}}(1/z^*)$ for a polynomial matrix [28]. The resulting signals, i.e. $v_i[m] = \widetilde{F}_0(zW^i)v[m]$, are then decimated by a K-fold decimator, yielding $y_i[n] = v_i[Kn]$. Equalization is then carried out via a one-tap per subcarrier scheme, and the received symbols $\hat{x}_i[n]$ are given by $\hat{x}_i[n] = e_i y_i[n]$.

2.2. Polyphase matrix representation

The polyphase representation can be used to conveniently express the filter banks as a polyphase matrix [29,30], which will prove to be highly useful in the following sections. We shall assume that D is a multiple of K and M, i.e. $D = k_1K$ and $D = k_2M$, where k_1 and k_2 are two integers. Let us consider the polyphase representation of $F_0(zW^i)$, $i = 0, \ldots, M-1$, i.e.

$$F_0(zW^i) = \sum_{k=0}^{K-1} z^k G_{k,i}(z^K),$$

where

$$G_{k,i}(z) = \sum_{n=0}^{D/K-1} f_0[Kn+k]W^{i(Kn+k)}z^n. \tag{1}$$

We then define the $K \times M$ transmitting polyphase matrix $\boldsymbol{G}(z)$ as a polynomial matrix whose (k,i)-th entry is given by $[\boldsymbol{G}(z)]_{k,i} = G_{k,i}(z)$.

The transmitting polyphase matrix $\boldsymbol{G}(z)$ can be factorized as described here, using the ideas presented in [31]. Let $\boldsymbol{g}_i(z)$ be the i-th column of $\boldsymbol{G}(z)$. From (1), $\boldsymbol{g}_i(z)$ can be expressed as

$$\boldsymbol{g}_i(z) = \widetilde{\boldsymbol{L}}_0(z)\boldsymbol{f}_i, \tag{2}$$

where $\widetilde{\boldsymbol{L}}_0(z) = [\boldsymbol{I}_K \; z\boldsymbol{I}_K \; \ldots \; z^{D/K-1}\boldsymbol{I}_K]$ and $\boldsymbol{f}_i = [f_0[0]W^{-0i} \; \ldots \; f_0[D-1]W^{-(D-1)i}]^{\mathrm{T}}$. Using the fact that $W^{M+l} = W^l$, we can write

$$\boldsymbol{f}_i = \boldsymbol{\Lambda}_f \boldsymbol{L}_1^{\mathrm{T}} \begin{bmatrix} W^{-0i} \\ \vdots \\ W^{-(M-1)i} \end{bmatrix}, \tag{3}$$

where $\boldsymbol{\Lambda}_f = \mathrm{diag}(f_0[0], \ldots, f_0[D-1])$ and

$$\boldsymbol{L}_1 = \underbrace{[\boldsymbol{I}_M \; \boldsymbol{I}_M \; \ldots \; \boldsymbol{I}_M]}_{D/M \text{ times}}.$$

From (2) and (3), $\boldsymbol{G}(z)$ can thus be factorized as follows:

$$\boldsymbol{G}(z) = [\boldsymbol{g}_0(z) \; \ldots \; \boldsymbol{g}_{M-1}(z)] = \widetilde{\boldsymbol{L}}_0(z)\boldsymbol{\Lambda}_f\boldsymbol{L}_1^{\mathrm{T}}\boldsymbol{W}^*,$$

where $\boldsymbol{W}$ is the DFT matrix, i.e. $[\boldsymbol{W}]_{i,k} = W^{ik}$. Note that it is convenient to express $\boldsymbol{G}(z)$ as

$$\boldsymbol{G}(z) = \widetilde{\boldsymbol{U}}(z)\boldsymbol{W}^*, \tag{4}$$

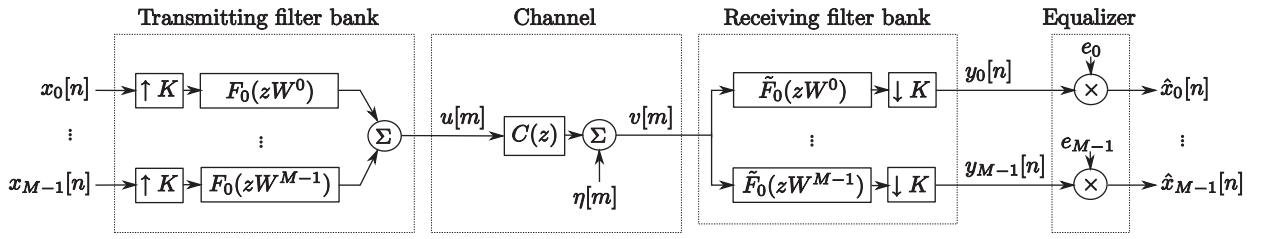

Fig. 1. The proposed PR DFT filter bank transceiver.

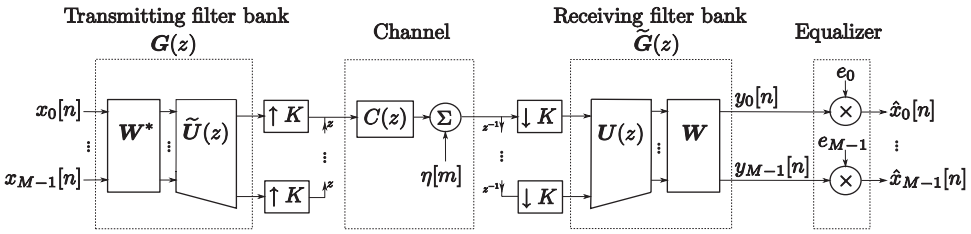

Fig. 2. Polyphase representation of the proposed transceiver.

where

$$\boldsymbol{U}(z) \triangleq \boldsymbol{L}_1 \boldsymbol{\Lambda}_f \boldsymbol{L}_0(z). \tag{5}$$

In the case of the receiving filter bank, a factorization similar to (4) can be established. We can show that the receiving polyphase matrix is given by $\widetilde{\boldsymbol{G}}(z) = \boldsymbol{W}\boldsymbol{U}(z)$. Using the transmitting and receiving polyphase matrices and with the help of the noble identities, the proposed filter bank transceiver illustrated in Fig. 1 can be represented as shown in Fig. 2.

In this work, we assume that the DFT filter banks in the proposed transceiver are paraunitary. The polyphase matrix of a paraunitary DFT filter bank satisfies the following relation:

$$\widetilde{\boldsymbol{G}}(z)\boldsymbol{G}(z) = \boldsymbol{I}_M. \tag{6}$$

In the presence of an ideal channel, i.e. with $C(z) = 1$ and $\eta[m] = 0$, we thus have $y_i[n] = x_i[n-d]$, where d is an integer delay. Such property is referred to as PR and is a direct consequence of the paraunitaryness of the system [28]. The design of paraunitary (and thus, PR) DFT filter banks is fully discussed in Sections 3 and 4.

3. Parametrization of the prototype filter

We define in this section the necessary mathematical relations to parametrize the prototype filter coefficients $f_0[m]$ such that the transmitting polyphase matrix $\boldsymbol{G}(z)$ is paraunitary and, thus, characterized by the PR property. The design of the prototype filter itself is addressed in Section 4. The parametrization requires that D, the prototype filter length, be a multiple of P, where P is defined as the least common multiple of M and K. We also define the quantities J and L as $J \triangleq P/M$ and $L \triangleq P/K$, respectively.

3.1. The two-step parametrization method

From (6), since $\boldsymbol{W}\boldsymbol{W}^* = \boldsymbol{I}_M$, one can observe that the paraunitaryness of $\boldsymbol{G}(z)$ can be guaranteed by letting $\boldsymbol{U}(z)$ to be paraunitary. The matrix $\boldsymbol{U}(z)$, defined in (5), exhibits a particular structure. Each entry of $\boldsymbol{U}(z)$, denoted by $U_{i,k}(z)$, $i = 0,\ldots,M-1$, $k = 0,\ldots,K-1$, is given by (see Appendix A for a proof):

$$U_{i,k}(z) = z^{-\alpha_{i,k}} G_{\beta_{i,k}}(z^L), \tag{7}$$

where $G_{\beta_{i,k}}(z)$ is the P-fold polyphase component of $f_0[m]$, i.e.

$$G_{\beta i,k}(z) \triangleq \sum_{n=0}^{D/P-1} f_0[Pn + \beta_{i,k}] z^{-n},$$

$\beta_{i,k} \triangleq \alpha_{i,k}K + k$, and $\alpha_{i,k} \in \{0,\ldots,L-1\}$ is an integer that depends on (i,k). As specified in Appendix A, $\alpha_{i,k}$ must satisfy the congruence relation[1]

$$\alpha_{i,k}K + k \equiv i \,(\mathrm{mod}\, M). \tag{8}$$

Note that $\alpha_{i,k}$ may—or may not—exist depending on the given (i,k). When $\alpha_{i,k}$ does not exist, we have $U_{i,k}(z) = 0$.

As an aside, let us now prove the critical importance of over-interpolation, i.e. having $K > M$, for the PR property to be feasible in a DFT filter bank. When $M = K$ (implying that $P = M$ and $L = 1$), (8) can only be satisfied for $i = k$, in which case we have $\alpha_{i,k} = 0$. The matrix $\boldsymbol{U}(z)$ is thus diagonal with the following entries:

$$U_{i,i}(z) = G_i(z), \quad i = 0,\ldots,M-1.$$

To satisfy the PR property, i.e. $\boldsymbol{U}(z)\widetilde{\boldsymbol{U}}(z) = \boldsymbol{I}_M$, we must have

$$G_i(z)\widetilde{G}_i(z) = 1,$$

which is only possible if $f_0[m] = 1$ for $m = 0,\ldots,M-1$. Accordingly, the only possible choice for $\boldsymbol{U}(z)$ is the identity matrix $\boldsymbol{I}_M$. This situation is that of OFDM, where the "prototype filter" is a rectangular window. Overlapping non-rectangular windows, such as the ones in DFT filter banks, can have the PR property only if over-interpolation is allowed.

The parametrization of $f_0[m]$ is based on the idea that if we can generate a polyphase matrix $\boldsymbol{U}(z;\boldsymbol{\theta})$ which is paraunitary, then we can find the parametrized filter coefficients $f_0[m;\boldsymbol{\theta}]$ via the relation in (7). We thus proceed in two steps:

(1) From a vector of parameters $\boldsymbol{\theta} \in \mathbb{R}^S$, we compute a polyphase matrix $\boldsymbol{U}(z;\boldsymbol{\theta})$ such that it is paraunitary and obeys the structure in (7). This operation can be represented by the mapping p, which is defined as

$$p : \mathbb{R}^S \longrightarrow \mathscr{U}; \quad \boldsymbol{\theta} \overset{p}{\longmapsto} \boldsymbol{U}(z;\boldsymbol{\theta}),$$

where $\mathscr{U}$ is the set of all $M \times K$ paraunitary matrices which comply with the form outlined in (7).

[1] We say that two integers a and b are congruent modulo M, denoted here by $a \equiv b \,(\mathrm{mod}\, M)$, if and only if $a - b$ is divisible by M.

(2) Using the relation in (7), we obtain the filter coefficients $f_0[m;\theta]$ by inspecting the entries of $\boldsymbol{U}(z;\boldsymbol{\theta})$. Formally, this relation can be represented by the mapping q, given by

$$q:\mathscr{U}\longrightarrow\mathbb{R}^D;\quad \boldsymbol{U}(z;\boldsymbol{\theta})\overset{q}{\longmapsto}\boldsymbol{f}_0(\boldsymbol{\theta}),$$

where $\boldsymbol{f}_0(\boldsymbol{\theta})$ denotes the vector of the parametrized filter coefficients, i.e.

$$\boldsymbol{f}_0(\boldsymbol{\theta})=[f_0[0;\boldsymbol{\theta}]\ \ \ldots\ \ f_0[D-1;\boldsymbol{\theta}]]^{\mathrm{T}}.$$

In short, the filter coefficients are obtained via the composition of the mappings p and q, i.e.

$$\boldsymbol{f}_0(\boldsymbol{\theta})=q\circ p(\boldsymbol{\theta}).$$

Once a suitable polyphase matrix $\boldsymbol{U}(z;\boldsymbol{\theta})$ has been obtained via Step 1, finding the corresponding filter coefficients, i.e. Step 2, is straightforward. The proper mapping is given by (7). However, Step 1 requires a less direct approach, as summarized here. An arbitrary paraunitary matrix, which we denote by $\boldsymbol{V}(z;\boldsymbol{\theta})$, can be parametrized using a dyadic-based factorization [32]. Unfortunately, the entries of such matrix will not correspond to the proper polyphase components as given in (7). While preserving its paraunitaryness, $\boldsymbol{V}(z;\boldsymbol{\theta})$ must thus be transformed so that its entries are compatible with those of $\boldsymbol{U}(z;\boldsymbol{\theta})$. The exact relation between $\boldsymbol{V}(z;\boldsymbol{\theta})$ and $\boldsymbol{U}(z;\boldsymbol{\theta})$ depends on whether M and K are coprime or not. Both situations are considered below.

3.2. Parametrization of the polyphase matrix for M and K coprime

Let us first consider the case where M and K are coprime, i.e. we have $L=M$ and $J=K$. We first compute a $L\times J$ paraunitary matrix $\boldsymbol{V}(z;\boldsymbol{\theta})$ using the following dyadic-based factorization [28,32]:

$$\boldsymbol{V}(z;\boldsymbol{\theta})=\prod_{l=0}^{D/P-3}\boldsymbol{A}(z;\boldsymbol{\theta}_l)\prod_{l=D/P-2}^{D/P+J-4}\boldsymbol{B}(\boldsymbol{\theta}_l),\tag{9}$$

where

$$\boldsymbol{\Gamma}=[\boldsymbol{I}_L\ \ \boldsymbol{0}_{L\times(J-L)}],$$

$$\boldsymbol{A}(z;\boldsymbol{\theta}_l)=\boldsymbol{I}_J-\frac{\boldsymbol{\theta}_l\boldsymbol{\theta}_l^{\mathrm{T}}}{\boldsymbol{\theta}_l^{\mathrm{T}}\boldsymbol{\theta}_l}+z^{-1}\frac{\boldsymbol{\theta}_l\boldsymbol{\theta}_l^{\mathrm{T}}}{\boldsymbol{\theta}_l^{\mathrm{T}}\boldsymbol{\theta}_l},$$

$$\boldsymbol{B}(\boldsymbol{\theta}_l)=\boldsymbol{I}_J-2\frac{\boldsymbol{\theta}_l\boldsymbol{\theta}_l^{\mathrm{T}}}{\boldsymbol{\theta}_l^{\mathrm{T}}\boldsymbol{\theta}_l},$$

and $\boldsymbol{\theta}_l$ are J-length vectors given by

$$\boldsymbol{\theta}_l=[1\ \ \theta_{l(J-1)}\ \ \theta_{l(J-1)+1}\ \ \ldots\ \ \theta_{l(J-1)+J-2}]^{\mathrm{T}}.$$

The entries of $\boldsymbol{\theta}_l$ are taken from the vector of parameters $\boldsymbol{\theta}=[\theta_0\ \ldots\ \theta_{S-1}]^{\mathrm{T}}$ with $S=(D/P+J-3)(J-1)$. When M and K are coprime, we can observe that, regardless of i and k, there always exists an integer $\alpha_{i,k}\in\{0,\ldots,L-1\}$ such that (8) is satisfied. In this case, each entry of $\boldsymbol{U}(z)$ is non-zero. However, we cannot simply let $\boldsymbol{U}(z;\boldsymbol{\theta})$ to be equal to the paraunitary matrix $\boldsymbol{V}(z;\boldsymbol{\theta})$ due to the terms $z^{-\alpha_{i,k}}$ and z^L in (7). In general, the structure of $\boldsymbol{U}(z;\boldsymbol{\theta})$ is not compatible with that of $\boldsymbol{V}(z;\boldsymbol{\theta})$. We thus have to transform $\boldsymbol{V}(z;\boldsymbol{\theta})$ such that the paraunitaryness is preserved and its entries can be mapped directly to those given in (7).

In order to find a suitable transformation for $\boldsymbol{V}(z;\boldsymbol{\theta})$, as proposed in [33], we consider two paraunitary matrices $\boldsymbol{D}_0(z)$ and $\boldsymbol{D}_1(z)$ such that

$$\boldsymbol{D}_0(z)=\mathrm{diag}([z^{\alpha_{0,0}}\ \ z^{\alpha_{1,0}}\ \ \ldots\ \ z^{\alpha_{L-1,0}}]),$$

$$\boldsymbol{D}_1(z)=\mathrm{diag}([z^{\alpha_{0,0}}\ \ z^{\alpha_{0,1}}\ \ \ldots\ \ z^{\alpha_{0,J-1}}]).$$

By pre-multiply and post-multiplying $\boldsymbol{U}(z)$ by $\boldsymbol{D}_0(z)$ and $\boldsymbol{D}_1(z)$, respectively, we can show that

$$[\boldsymbol{D}_0(z)\boldsymbol{U}(z)\boldsymbol{D}_1(z)]_{i,k}=z^{\bar{\alpha}_{i,k}}G_{\beta_{i,k}}(z^L),$$

where $\bar{\alpha}_{i,k}=\alpha_{i,0}+\alpha_{0,k}-\alpha_{i,k}$. Let us consider two expressions derived from (8), where we, respectively, let $(i,k)=(0,k)$ and $(i,k)=(i,0)$. Using the properties of congruences [34], adding these two expressions together and subtracting from it relation (8) yield

$$(\alpha_{i,0}+\alpha_{0,k}-\alpha_{i,k})J\equiv 0\,(\mathrm{mod}\ L).$$

The above expression indicates that $\bar{\alpha}_{i,k}$ can only take two different values, 0 or L, since we have $0\leqslant\alpha_{i,k}\leqslant L-1$ for all i and k. Based on this information, we note that the entries of $\boldsymbol{D}_0(z)\boldsymbol{U}(z)\boldsymbol{D}_1(z)$ are solely given in terms of z^L. Hence, we can now let

$$\boldsymbol{D}_0(z)\boldsymbol{U}(z;\boldsymbol{\theta})\boldsymbol{D}_1(z)=\boldsymbol{V}(z^L;\boldsymbol{\theta}),$$

or, equivalently,

$$\boldsymbol{U}(z;\boldsymbol{\theta})=\widetilde{\boldsymbol{D}}_0(z)\boldsymbol{V}(z^L;\boldsymbol{\theta})\widetilde{\boldsymbol{D}}_1(z).\tag{10}$$

Since $\boldsymbol{V}(z;\boldsymbol{\theta})$ is paraunitary, then so is $\boldsymbol{U}(z;\boldsymbol{\theta})$, as the product of two paraunitary matrices preserves paraunitaryness [28].

In essence, we have shown that the first step of the parametrization, i.e. to obtain a proper paraunitary matrix $\boldsymbol{U}(z;\boldsymbol{\theta})$, first consists in generating a generic paraunitary matrix $\boldsymbol{V}(z;\boldsymbol{\theta})$ via the dyadic-based factorization given in (9). As shown in (10), we then apply a transformation to $\boldsymbol{V}(z;\boldsymbol{\theta})$ to make its entries compatible with those of $\boldsymbol{U}(z;\boldsymbol{\theta})$. Once $\boldsymbol{U}(z;\boldsymbol{\theta})$ has been obtained, we may easily carry out the second step of the parametrization by retrieving the filter coefficients via mapping (7).

3.3. Parametrization of the polyphase matrix for M and K non-coprime

When M and K are not coprime, it is not always possible to find an integer $\alpha_{i,k}$ which satisfies (8) for a given (i,k). Hence, $\boldsymbol{U}(z)$ will have zero and non-zero entries. It turns out that the paraunitaryness of $\boldsymbol{U}(z)$ is equivalent to the paraunitaryness of $L\times J$ submatrices $\boldsymbol{U}_l(z)$, $l=0,\ldots,K/J-1$, of $\boldsymbol{U}(z)$ [33]. These submatrices are constructed as follows:

$$\boldsymbol{U}_l(z)=\begin{bmatrix}U_{l,l}(z) & \ldots & U_{l,l+(J-1)K/J}\\ U_{l+M/L,l}(z) & \ldots & U_{l+M/L,l+(J-1)K/J}\\ \vdots & \ddots & \vdots\\ U_{l+(L-1)M/L,l}(z) & \ldots & U_{l+(L-1)M/L,l+(J-1)K/J}\end{bmatrix},\tag{11}$$

where each entry is given by (7).

Notice that, for any entry of $\boldsymbol{U}_l(z)$, the congruence relation (8) can be written as

$$\alpha_{i,k}K + l + k\frac{K}{J} \equiv l + i\frac{M}{L} (\text{mod } M),$$

which is equivalent to

$$\alpha_{i,k}J + k \equiv i \,(\text{mod } M),$$

since, by definition, $K/J = M/L$. By comparing the above expression with (8), we may conclude that the distribution of the term $\alpha_{i,k}$ in the $L \times J$ matrix $\boldsymbol{U}_l(z)$ is identical to the one found in the coprime case. Hence, the same transformation as in (10) can be used, and we can write

$$\boldsymbol{U}_l(z;\boldsymbol{\theta}) = \widetilde{\boldsymbol{D}}_0(z)\boldsymbol{V}_l(z^L;\boldsymbol{\theta})\widetilde{\boldsymbol{D}}_1(z), \tag{12}$$

where $\boldsymbol{V}_l(z^L;\boldsymbol{\theta})$ is a $L \times J$ paraunitary matrix, generated via the same dyadic-based factorization used in the coprime case.

The procedure to obtain $\boldsymbol{f}_0(\boldsymbol{\theta})$ can now be generalized as follows. Initially, the factorization theorem of paraunitary matrices, i.e. (9), is used to generate K/J matrices $\boldsymbol{V}_l(z;\boldsymbol{\theta})$. These matrices are then mapped to $\boldsymbol{U}_l(z;\boldsymbol{\theta})$ via the transformation shown in (12). Finally, we retrieve the filter coefficients by inspecting each entry of $\boldsymbol{U}_l(z;\boldsymbol{\theta})$, using the information contained in (11) and in (7).

4. Design of the prototype filter

In this section, we use the parametrization of the filter coefficients described in Section 3 to propose a design methodology for PR DFT filter banks with good spectral containment.

4.1. Optimization problem

In order to provide good spectral containment, among all parameter vectors $\boldsymbol{\theta}$, it is desirable to select the one that minimizes the stopband energy of $f_0[m;\boldsymbol{\theta}]$. The prototype filter design problem can thus be cast as the following unconstrained optimization problem:

$$\boldsymbol{\theta}_0 = \arg\min_{\boldsymbol{\theta}} J(\boldsymbol{\theta}), \tag{13}$$

where the cost function, $J(\boldsymbol{\theta})$, corresponds to the stopband energy of the prototype filter. The stopband energy can be expressed as

$$J(\boldsymbol{\theta}) = \int_{\omega_s}^{2\pi-\omega_s} |F_0(\mathrm{e}^{\mathrm{j}\omega};\boldsymbol{\theta})|^2 \,\mathrm{d}\omega, \tag{14}$$

where $F_0(\mathrm{e}^{\mathrm{j}\omega};\boldsymbol{\theta})$ represents the discrete-time Fourier transform (DTFT) of $f_0[m;\boldsymbol{\theta}]$, i.e.

$$F_0(\mathrm{e}^{\mathrm{j}\omega};\boldsymbol{\theta}) = \sum_{m=0}^{D-1} f_0[m;\boldsymbol{\theta}]\mathrm{e}^{-\mathrm{j}\omega m},$$

and ω_s denotes the stopband frequency, which is given by

$$\omega_s = \frac{\pi}{M}.$$

Note that this approach is similar to the one suggested in [35] for unstructured filter banks. Thanks to the parametrization of $f_0[m]$, one is certain that $f_0[m;\boldsymbol{\theta}]$ will always yield a PR prototype filter regardless of the outcome of the minimization process. It is not necessary to constrain the passband of the prototype filter to be flat to obtain a good frequency response. Due to the paraunitaryness of $\boldsymbol{G}(z)$, one can show, using the power complementary property, that the passband region of $|F_0(\mathrm{e}^{\mathrm{j}\omega};\boldsymbol{\theta})|^2$ will be constant, even if the cost function does not explicitly take this into account [28].

Minimization of the cost function can be carried out using any algorithm suitable for large-scale non-linear unconstrained optimization problems. In this work, we propose to use the Broyden–Fletcher–Goldfarb–Shanno (BFGS) algorithm, which is appropriate for solving such problems [36]. To implement the BFGS algorithm, we employ the L-BFGS-B (Bound constrained[2] Limited memory BFGS) software [37,38]. The required gradient of the cost function, $\nabla J(\boldsymbol{\theta})$, can be approximated numerically using the standard difference-based approach. The i-th entry of the gradient is thus obtained as follows:

$$[\nabla J(\boldsymbol{\theta})]_i \approx \frac{J(\boldsymbol{\theta} + \varepsilon \boldsymbol{e}_i) - J(\boldsymbol{\theta})}{\varepsilon},$$

where ε is a small positive real number, and $\boldsymbol{e}_i$ is an all-zero vector, except at the i-th entry where it is one. Note that the convergence towards a global minimum cannot be guaranteed since the cost function is not convex. To find a "good" minimum, the algorithm should be run several times with a different set of initial values, and the solution yielding the lowest minimum should be kept.

4.2. Computation of the stopband energy

The cost function in (14) can be evaluated without resorting to approximate numerical integration methods. The main idea is to consider the autocorrelation of the impulse response of the prototype filter [39], defined for $-D+1 \leqslant \tau \leqslant D-1$ as

$$r_f[\tau;\boldsymbol{\theta}] \triangleq \sum_{m=0}^{D-1} f_0[m;\boldsymbol{\theta}] f_0[m+\tau;\boldsymbol{\theta}]. \tag{15}$$

Using basic properties of the DTFT [40], the cost function can be re-written in terms of the autocorrelation function as follows:

$$J(\boldsymbol{\theta}) = \int_{\omega_s}^{2\pi-\omega_s} R_f(\mathrm{e}^{\mathrm{j}\omega};\boldsymbol{\theta}) \,\mathrm{d}\omega, \tag{16}$$

where $R_f(\mathrm{e}^{\mathrm{j}\omega};\boldsymbol{\theta})$ is the DTFT of $r_f[\tau;\boldsymbol{\theta}]$, i.e.

$$R_f(\mathrm{e}^{\mathrm{j}\omega};\boldsymbol{\theta}) = \sum_{\tau=-D+1}^{D-1} r_f[\tau;\boldsymbol{\theta}]\mathrm{e}^{-\mathrm{j}\omega\tau}. \tag{17}$$

Finally, substituting (17) in (16) and carrying out the integral yields

$$J(\boldsymbol{\theta}) = \sum_{\tau=0}^{D-1} b[\tau] r_f[\tau;\boldsymbol{\theta}], \tag{18}$$

[2] Despite its name, L-BFGS-B is also suitable for unconstrained problem, like the one in (13).

Table 1
Computation of the autocorrelation function using the FFT

Instructions	Flops
1: Let $D' = 2^E$, where $E = \lceil \log_2 D \rceil + 1$	Negligible
2: Let $B[k]$ be the D'-point FFT of $b[\tau]$ (this can be computed offline)	
3: Compute $F_0[k]$, the D'-point FFT of $f_0[m;\boldsymbol{\theta}]$, by zero-padding the sequence	$5D' \log_2 D'$
4: Let $H[k] = \lvert F_0[k] \rvert^2$ for $k = 0, \ldots, D'-1$	$3D'$
5: Compute $J(\boldsymbol{\theta}) = \frac{1}{D'} \sum_{k=0}^{D'-1} B[k] H^*[k]$	$2D'$

where

$$b[\tau] = \begin{cases} 1 - \omega_s/\pi & \text{if } \tau = 0, \\ -\dfrac{2}{\pi\tau}\sin(\tau\omega_s) & \text{if } \tau = 1, \ldots, D-1, \\ 0 & \text{elsewhere.} \end{cases}$$

The stopband energy can thus be computed analytically via a finite sum, as shown in (18).

Computing the stopband energy of $f_0[m;\boldsymbol{\theta}]$ can be a costly operation if one implements (15) and (18) directly. In fact, even if we take into account the symmetry of $r_f[\tau;\boldsymbol{\theta}]$, i.e. $r_f[-\tau;\boldsymbol{\theta}] = r_f[\tau;\boldsymbol{\theta}]$, its computation requires $2D^2$ flops (floating point operations). For a 512-tap filter, this amounts to 0.52 Mflops, which makes the optimization problem a relatively time-consuming and a resource-demanding process. Instead, we can carry out the computation in the frequency domain, as described in Table 1, where a FFT-based algorithm is presented. If we consider again a 512-tap filter, the FFT-based method necessitates 0.05 Mflops, a reduction by almost a factor of 10 compared to the direct approach. Computing the stopband energy via the FFT thus decreases the computational burden of the optimization problem significantly.

The design method presented in this section is illustrated in Fig. 3.

5. Channel equalization

Many schemes have been proposed to equalize the channel in a DFT filter bank transceiver. Systems employing non-PR DFT filter banks usually rely on a set of DFEs which compensate for both the channel attenuations and the distortion introduced by the filter banks [26]. In PR DFT filter bank transceivers, the use of DFEs would be an overly complex solution since it is then unnecessary to mitigate the filter-bank-induced distortion.

As an alternative to the use of DFEs, a simple one-tap per subcarrier equalizer can be considered, as illustrated in Figs. 1 and 2. The computational complexity of the one-tap equalizer is minimal, requiring only one complex multiplication per subcarrier. To operate properly, however, the prototype filter must exhibit "good" spectral characteristics, i.e. a narrow passband, a sharp transition band and a high out-of-band rejection. Provided that these conditions can be satisfied, each subchannel can then be modelled as a simple complex gain which can be compensated by a single tap.

The equalizer coefficients e_i, $i = 0, \ldots, M-1$, can be computed from the channel impulse response $c[m]$. Using a zero-forcing approach, e_i corresponds to the inverse of the channel attenuation at frequency $\omega_i = 2\pi i/M$, i.e.

$$e_i = \frac{1}{C(e^{j2\pi i/M})}, \tag{19}$$

where $C(e^{j\omega})$ is the DTFT of $c[m]$.

6. Computer experiments

6.1. Prototype filter design

We first attempt to design a PR prototype filter using the steps outlined in Section 4. Various combinations of K, the upsampling factor, and D, the prototype filter length, are considered for a 128-subcarrier transceiver ($M = 128$). The frequency responses of the resulting filters are illustrated in Fig. 4. The stopband energy and the attenuation of the first sidelobe of these filters, representing important spectral features, are given in Table 2. Note that we normalize the total energy of the filters to 30 dBm.

From Table 2, we can conclude that, for a given number of subcarriers M, better spectral features are obtained if the upsampling factor K and the length of the prototype filter D are increased. However, one must be careful as a higher K will reduce the bandwidth efficiency of the system. Likewise, a higher D will introduce more latency in the system and increase its computational complexity. These factors must be balanced carefully in order to maintain a low latency, a low computational complexity, and a high bandwidth efficiency while benefiting from good spectral features.

Fig. 5 shows the frequency responses of an OFDM prototype filter with $M = 128$ and a PR prototype filter with $M = 128$, $K/M = 1.25$ and $D/M = 20$. Three key observations must be pointed out. We first note that the transition from passband to stopband, i.e. the rolloff, is much steeper with the PR DFT filter bank than with OFDM. Moreover, the stopband energy and the attenuation of the first sidelobe are, respectively, about 15 and 43 dB, whereas the stopband energy and the attenuation of the first sidelobe of the OFDM system are, respectively, 24 and 13 dB. These observations confirm that PR DFT filter banks offer considerably better spectral containment than OFDM.

If the prototype filter is not subject to the PR constraint, as it is the case in filtered multitone (FMT) [18], the spectral containment can be further improved. We show in Fig. 6 an example of a non-PR (or near-PR) prototype filter which is designed with the windowing method, as proposed in [23]. We follow the advice given in [23], and, for best performance, we employ a Kaiser window with parameter $\beta = 8.96$ and a cutoff frequency of $\omega_c = \pi(1+\delta)/K$, $\delta = 0.15$. Despite its impressive spectral properties,[3] the non-PR system requires the use

[3] Typically, FMT systems employ shorter filters with $D/M = 10$ [18], whereas our solution requires 20 taps per subchannel due to the PR constraint which needs to be satisfied.

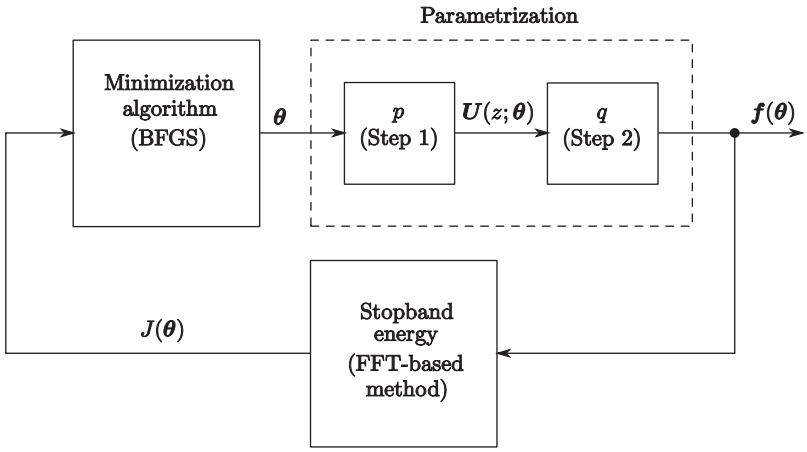

Fig. 3. Outline of the prototype filter design process.

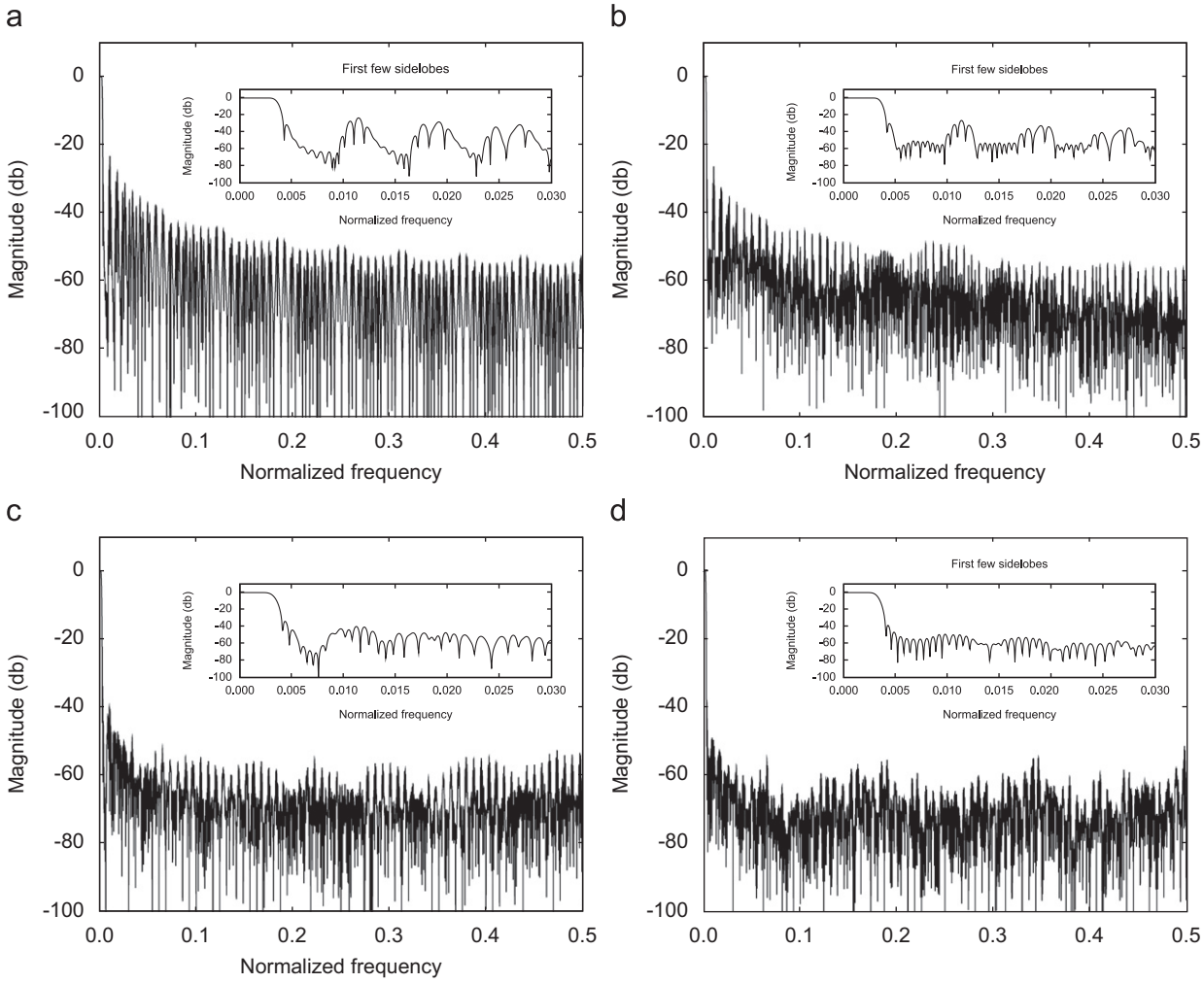

Fig. 4. Frequency responses of PR DFT filter bank prototype filters: (a) $M = 128$, $K/M = 1.125$ and $D/M = 18$; (b) $M = 128$, $K/M = 1.125$ and $D/M = 27$; (c) $M = 128$, $K/M = 1.25$ and $D/M = 20$; and (d) $M = 128$, $K/M = 1.25$ and $D/M = 30$.

Table 2
Spectral features of several PR prototype filters

M	K/M	D/M	Stopband energy (dBm)	Attenuation of the first sidelobe (dB)
128	1.125	18	26	−29
128	1.125	27	23	−32
128	1.25	20	15	−43
128	1.25	30	10	−49

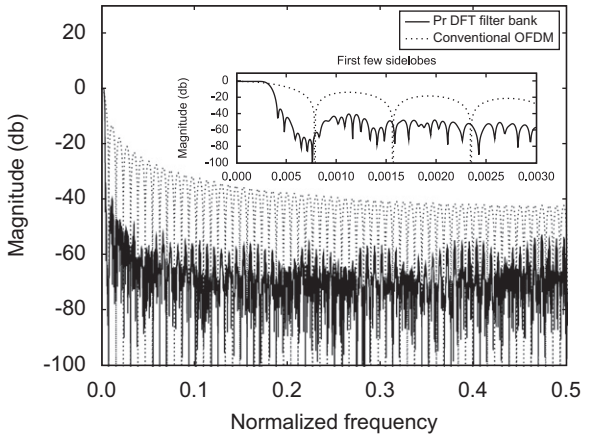

Fig. 5. Frequency responses of the PR DFT filter bank with $M = 128$, $K/M = 1.25$ and $D/M = 20$ and of the OFDM prototype filter with $M = 128$.

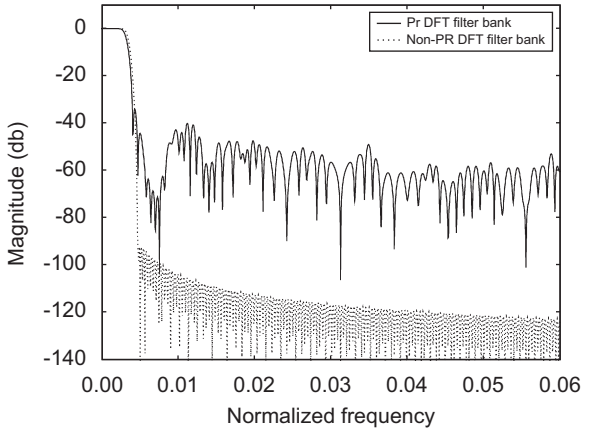

Fig. 6. Frequency responses of the first few sidelobes of the PR and non-PR DFT filter banks with $M = 128$, $K/M = 1.25$ and $D/M = 20$.

of a computationally demanding equalization scheme, in the form of per-subcarrier DFEs, to mitigate the interference due to the non-PR of the filter banks [26]. As we will see below, the performance of non-PR systems using simple one-tap equalizers is unacceptable.

6.2. Achievable bit rates

We now assess the performance of our proposed system in a DSL-like environment. A sampling rate f_s of

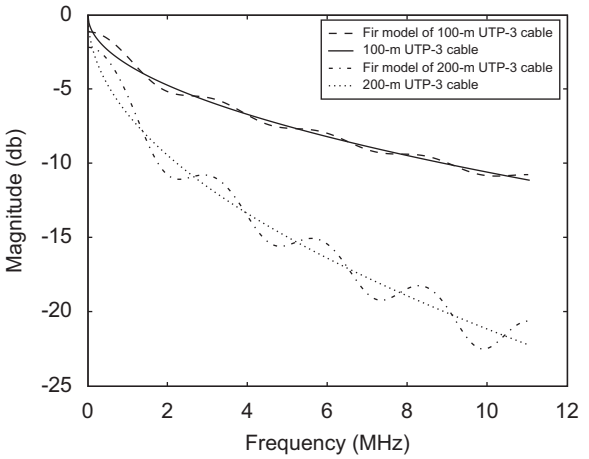

Fig. 7. Frequency responses of the channels modelling a 100- and a 200-m UTP-3 cable.

Table 3
International amateur radio frequency bands (below 11 MHz)

Category	Start (MHz)	End (MHz)
160 m	1.81	2.00
80 m	3.50	3.80
40 m	7.00	7.10
30 m	10.10	10.15

22.08 MHz is selected. We consider two local loops, consisting in a 100- and a 200-m UTP-3 copper wire, whose frequency response is taken from [18]. In DSL, the impulse response of the local loops is normally infinite, and a time-domain equalizer is usually employed to shorten the channel to a finite length [41]. However, for simulation purposes, the frequency response of the local loops is conveniently approximated via two 17-tap FIR filters (i.e. Q, the channel length, is 17) as shown in Fig. 7.

Two different noisy conditions are considered, corresponding to additive white Gaussian noise (AWGN) and RFI. To facilitate comparison, both types of noise are set to the same power. RFI can be modelled as a narrowband noise located in one of the possible frequency bands reserved for amateur radio usage, which are enumerated in Table 3 [42]. The power is generally limited to 400 W or 56 dBm [42]. Under unfavourable conditions, e.g. when the antenna and the local loop are separated by 10 m and run parallel to each other, an ingress power of about −4 dB can be measured [42]. We thus consider here a −4 dBm

narrowband noise, centred at 1.8113 MHz and located in the first amateur radio band. The narrowband noise is generated using a second-order autoregressive process, and its power spectral density (PSD) is illustrated in Fig. 8.

Performance is evaluated by computing the theoretical achievable bit rate in order to maintain an error probability of 10^{-7}. To do so, we first determine the number of bits b_i allocated for each subcarrier using the relation proposed in [43]:

$$b_i = \log_2\left(1 + \frac{\mathrm{SNR}_i}{\Gamma}\right), \quad i = 0, \ldots, M-1, \tag{20}$$

where SNR_i is the signal-to-noise ratio at the output of the i-th subcarrier and Γ is the SNR "gap". By assuming an error probability of 10^{-7} and the use of coded QAM symbols, the gap can be obtained as follows [43]:

$$\Gamma = 9.8 + \gamma_{\mathrm{m}} - \gamma_{\mathrm{c}} \quad (\text{in dB}),$$

where γ_{m} is the margin, whose purpose is to ensure good performance under unforeseen conditions, and γ_{c} is the coding gain. Here, we select $\gamma_{\mathrm{m}} = \gamma_{\mathrm{c}}$ and $\Gamma = 9.8$. We also assume that the available power budget is divided equally among all subcarriers. Finally, the overall achievable bit rate is given by

$$R = \frac{f_s}{K} \sum_{i=0}^{M-1} b_i, \tag{21}$$

where K is the length of the transmitted multicarrier frame, taking into account the length of the cyclic prefix in the case of OFDM.

Fig. 9 shows the bit rate obtained by varying the signal power of the following transceivers: the proposed PR DFT filter bank transceiver, a similar transceiver using a

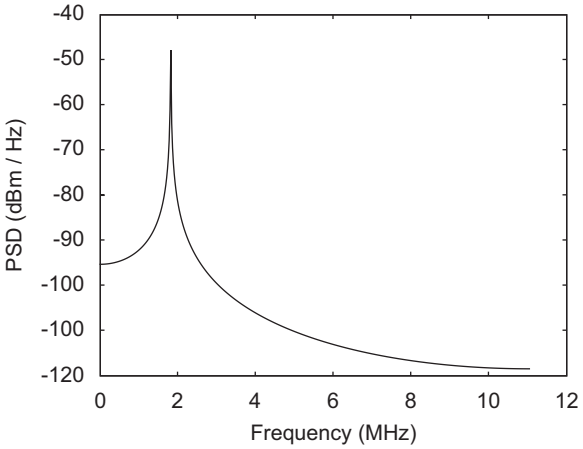

Fig. 8. Power spectral density of the radio frequency interference.

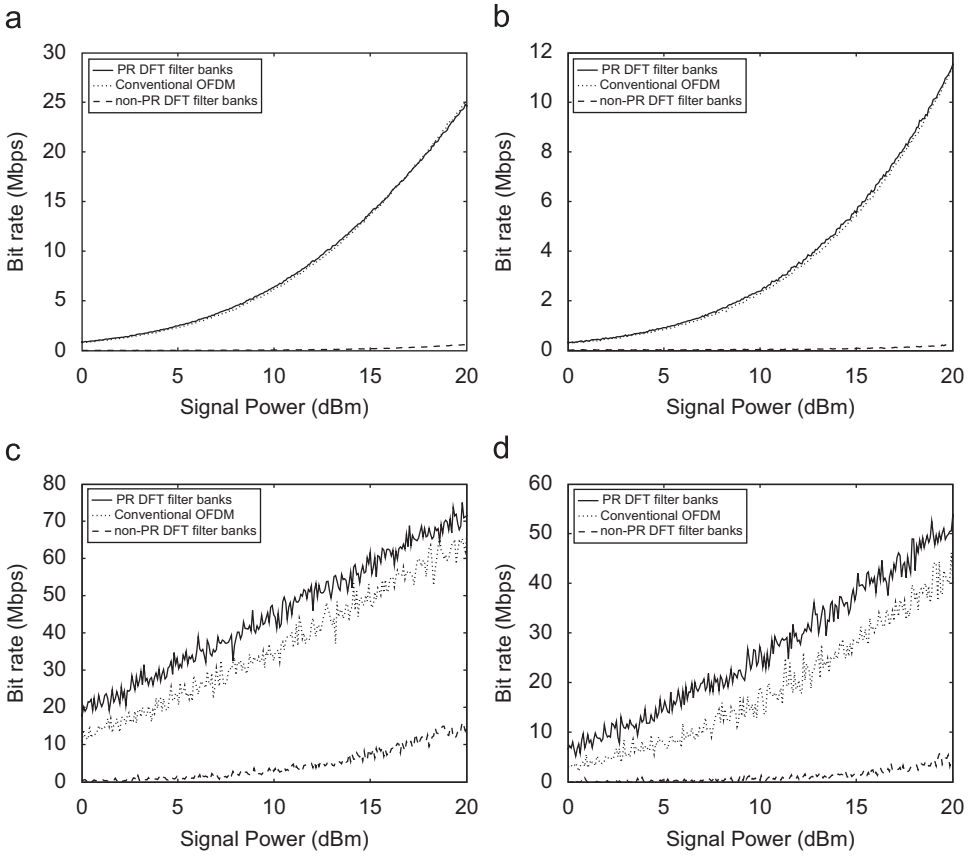

Fig. 9. Achievable bit rate of the OFDM system and the proposed transceiver with a PR and a non-PR prototype filter: (a) AWGN and 100-m loop; (b) AWGN and 200-m loop; (c) RFI and 100-m loop; and (d) RFI and 200-m loop.

non-PR prototype filter, and an OFDM system. We employ the PR and the non-PR prototype filters that are depicted in Fig. 6.

Fig. 9 confirms that a non-PR prototype filter is not suitable for one-tap equalization schemes, since the achievable bit rate of the transceiver employing such a filter is very poor. As reported in [26], non-PR filter banks generally produce too much ISI to be mitigated by a single tap. The PR DFT filter bank transceiver, however, exhibits a performance comparable to that of the OFDM system when AWGN contaminates the communication channel. Under a RFI impairment, the proposed PR DFT filter bank transceiver outperforms the OFDM system, with a difference of about 10 Mbps between the two.

6.3. Computational complexity

Implementing an over-interpolated DFT filter bank requires $5M\log_2 M + 2D$ flops per received frame of symbols according to the implementation described in [31]. Combined with the one-tap equalizer, the total number of flops is thus $5M\log_2 M + 2D + 6M$ if we assume that one complex multiplication is equivalent to six real ones. In contrast, the OFDM receiver necessitates $5M\log_2 M + 6M$ flops. Hence, by employing the PR prototype filter shown in Fig. 6, our proposed transceiver is approximately 2 times more complex than a conventional OFDM system. Depending on the situation, the increase in complexity can largely be offset by the increase in performance.

7. Conclusion

In this paper, we considered PR DFT filter banks for multicarrier transceivers. PR DFT filter banks were designed using a novel method, which was based in part on the parametrization of the impulse response of the prototype filter by a set of real parameters. The parametrization was carried out such that the resulting polyphase matrix of the DFT filter bank was paraunitary, which guaranteed that the PR property is satisfied. To select the proper set of real coefficients, we formulated the problem as an unconstrained optimization problem where the goal was to maximize the spectral containment of the filter bank, or, equivalently, to minimize the stopband energy of the prototype filter. The stopband energy was computed via the autocorrelation of the prototype filter's impulse response. Experimental results showed that the spectral containment of the resulting filter bank was considerably better than that of the OFDM system. It also turned out that the achievable bit rate of our proposed transceiver in a DSL-like environment contaminated by radio frequency interference was significantly higher than the bit rate achieved by an OFDM system.

As a follow-up to this work, we could investigate the use of other methods to solve the unconstrained optimization problem (13). We observed that designing a prototype filter using the BFGS algorithm posed some difficulties with $M > 128$ due to the number of parameters involved. We could, for instance, reduce the number of parameters in (9) by arbitrary assigning a fixed value to some of the vectors $\boldsymbol{\theta}_l$. Another possibility would be to consider other optimization strategies such as genetic algorithms [44].

Appendix A. Entries of the polyphase matrix $\boldsymbol{U}(z)$

We prove in this appendix that the entries of $\boldsymbol{U}(z)$ are given by (7), provided that $\alpha_{i,k}$, given in (8), exists. Let us first recall that $\boldsymbol{U}(z)$ can be written as

$$\boldsymbol{U}(z) = \boldsymbol{L}_1 \boldsymbol{\Lambda}_f \boldsymbol{L}_0(z).$$

Let us consider $M \times K$ matrices $\boldsymbol{F}_l$, $l = 0, \ldots, D/K - 1$, as a partition of $\boldsymbol{L}_1\boldsymbol{\Lambda}_f$, i.e.

$$[\boldsymbol{F}_0 \ \ \ldots \ \ \boldsymbol{F}_{D/K-1}] = \boldsymbol{L}_1 \boldsymbol{\Lambda}_f. \tag{22}$$

Then, the matrix $\boldsymbol{U}(z)$ in (4) can also be written as

$$\boldsymbol{U}(z) = [\boldsymbol{F}_0 \ \ \ldots \ \ \boldsymbol{F}_{D/K-1}]\boldsymbol{L}_0(z) = \sum_{l=0}^{D/K-1} \boldsymbol{F}_l z^{-l}. \tag{23}$$

Let us now consider the expression

$$l = nL + \alpha,$$

where $\alpha \in \{0, \ldots, L-1\}$ and $n \in \{0, \ldots, D/P - 1\}$. We can then re-write (23) as

$$\boldsymbol{U}(z) = \sum_{n=0}^{D/P-1} \sum_{\alpha=0}^{L-1} \boldsymbol{F}_{nL+\alpha} z^{-nL-\alpha}, \tag{24}$$

where, according to (22), we have

$$[\boldsymbol{F}_{nL+\alpha}]_{i,k} = \begin{cases} f_0[nP + \alpha K + k] & \text{if } \alpha K + k \equiv i \,(\text{mod } M), \\ 0 & \text{otherwise.} \end{cases}$$

We may notice that $[\boldsymbol{F}_{nL+\alpha}]_{i,k}$ can only be non-zero for a specific value of α since $\alpha K + k \equiv i \,(\text{mod } M)$ can only be satisfied for a given $\alpha \in \{0, \ldots, L-1\}$. We denote this value of α by $\alpha_{i,k}$. This implies that

$$\sum_{\alpha=0}^{L-1} [\boldsymbol{F}_{nL+\alpha}]_{i,k} = [\boldsymbol{F}_{nL+\alpha}]_{i,k},$$

and, using (24), we have

$$U_{i,k}(z) = z^{-\alpha} \sum_{n=0}^{D/P-1} [\boldsymbol{F}_{nL+\alpha}]_{i,k} z^{-nL}. \tag{25}$$

Finally, from (25), we can observe that if there exists $\alpha_{i,k} \in \{0, \ldots, L-1\}$ such that

$$\alpha_{i,k} K + k \equiv i \,(\text{mod } M),$$

then

$$U_{i,k}(z) = z^{-\alpha_{i,k}} \sum_{n=0}^{D/P-1} f_0[nP + \alpha_{i,k} K + k] z^{-nL}.$$

Otherwise,

$$U_{i,k}(z) = 0.$$

Note that if $\alpha_{i,k}$ exists, we can show that it is unique.

References

[1] J.A.C. Bingham, Multicarrier modulation for data transmission: an idea whose time has come, IEEE Comm. Mag. 28 (5) (May 1990) 5–14.

[2] T. Starr, J.M. Cioffi, P.J. Silverman, Understanding Digital Subscriber Line Technology, Prentice-Hall, Englewood Cliffs, NJ, 1999.

[3] H. Liu, G. Li, OFDM-Based Broadband Wireless Networks: Design and Optimization, Wiley, New York, 2005.

[4] A.J. Coulson, Bit error rate performance of OFDM in narrowband interference with excision filtering, IEEE Trans. Wireless Comm. 5 (9) (September 2006) 2484–2492.

[5] A.R. Lindsey, Wavelet packet modulation for orthogonally multiplexed communication, IEEE Trans. Signal Process. 45 (5) (May 1997) 1336–1339.

[6] K.M. Wong, J. Wu, T.N. Davidson, Q. Jin, Wavelet packet division multiplexing and wavelet packet design under timing error effects, IEEE Trans. Signal Process. 45 (12) (December 1997) 2877–2890.

[7] L. Vangelista, N. Laurenti, Efficient implementations and alternative architectures for OFDM-OQAM systems, IEEE Trans. Comm. 49 (4) (April 2001) 664–675.

[8] M.A. Tzannes, M.C. Tzannes, J. Proakis, P.N. Heller, DMT systems, DWMT systems and digital filter banks, in: Proceedings of the IEEE International Conference on Communications, May 1994, pp. 311–315.

[9] A.D. Rizos, J.G. Proakis, T.Q. Nguyen, Comparison of DFT and cosine modulated filter banks in multicarrier modulation, in: Proceedings of the IEEE Global Telecommunications Conference, vol. 2, December 1994, pp. 687–691.

[10] S.D. Sandberg, M.A. Tzannes, Overlapped discrete multitone modulation for high speed copper wire communications, IEEE J. Sel. Areas Comm. 13 (9) (December 1995) 1571–1585.

[11] C.Y. Chen, S.M. Phoong, Zero forcing cosine modulated filter bank transceivers with cyclic prefix, in: Proceedings of the International Workshop on Spectral Methods and Multirate Signal Processing, September 2002.

[12] V. Couturier-Doux, J. Lienard, B. Conq, P. Gallay, Efficient implementation of discrete wavelet multitone in DSL communications, in: Proceedings of the EURASIP Conference on Video/Image Processing and Multimedia Communications, vol. 1, July 2003, pp. 393–398.

[13] B. Farhang-Boroujeny, Multicarrier modulation with blind detection capability using cosine modulated filter banks, IEEE Trans. Comm. 51 (12) (December 2003) 2057–2070.

[14] B. Farhang-Boroujeny, L. Lin, Analysis of post-combiner equalizers in cosine-modulated filterbank-based transmultiplexer systems, IEEE Trans. Signal Process. 51 (12) (December 2003) 3249–3262.

[15] B. Farhang-Boroujeny, L. Lin, Cosine modulated multitone for very high-speed digital subscriber lines, in: Proceedings of the IEEE International Conference on Acoustics, Speech, and Signal Processing, vol. 3, March 2005, pp. 345–348.

[16] G. Cherubini, E. Eleftheriou, S. Olcer, Filtered multitone modulation for VDSL, in: Proceedings of the IEEE Global Telecommunications Conference, vol. 2, December 1999, pp. 1139–1144.

[17] G. Cherubini, E. Eleftheriou, S. Oker, J.M. Cioffi, Filter bank modulation techniques for very high speed digital subscriber lines, IEEE Comm. Mag. 38 (5) (May 2000) 98–104.

[18] G. Cherubini, E. Eleftheriou, S. Olcer, Filtered multitone modulation for very high-speed digital subscriber lines, IEEE J. Sel. Areas Comm. 20 (5) (June 2002) 1016–1028.

[19] S.-M. Phoong, Y. Chang, C.-Y. Chen, DFT-modulated filterbank transceivers for multipath fading channels, IEEE Trans. Signal Process. 53 (1) (January 2005) 182–192.

[20] B. Borna, T.N. Davidson, Efficient filter bank design for filtered multitone modulation, in: Proceedings of the IEEE International Conference on Communications, vol. 1, June 2004, pp. 38–42.

[21] B. Borna, T.N. Davidson, Efficient design of FMT systems, IEEE Trans. Comm. 54 (5) (May 2006) 794–797.

[22] I. Berenguer, I.J. Wassell, FMT modulation: receiver filter bank definition for the derivation of an efficient implementation, in: Proceedings of the International OFDM Workshop, September 2002.

[23] A. Lim, H.H. Dam, S. Nordholm, Filter bank design for DFT based transmultiplexers, in: Proceedings of the Asia-Pacific Conference on Communications, October 2005, pp. 965–968.

[24] Y. Gao, Z. Gao, W. Zhu, X. Yang, The research on the design of filter banks in filtered multitone modulation, in: Proceedings of the IEEE Wireless Communications and Networking Conference, vol. 1, March 2005, pp. 584–588.

[25] A. Tonello, Time domain and frequency domain implementations of FMT modulation architectures, in: Proceedings of the IEEE International Conference on Acoustics, Speech and Signal Processing, vol. 4, May 2006, pp. 625–628.

[26] N. Benvenuto, S. Tomasin, L. Tomba, Equalization methods in OFDM and FMT systems for broadband wireless communications, IEEE Trans. Comm. 50 (9) (September 2002) 1413–1418.

[27] K. Kajita, H. Kobayashi, S. Muramatsu, A. Yamada, H. Kiya, A design method for oversampled paraunitary DFT filter banks using householder factorization, in: Proceedings of the European Signal Processing Conference, September 1996, pp. 192–195.

[28] P.P. Vaidyanathan, Multirate Systems and Filter Banks, Prentice-Hall, Englewood Cliffs, NJ, 1993.

[29] X.-G. Xia, New precoding for intersymbol interference cancellation using nonmaximally decimated multirate filterbanks with ideal FIR equalizers, IEEE Trans. Signal Process. 45 (10) (October 1997) 2431–2441.

[30] A. Scaglione, G.B. Giannakis, S. Barbarossa, Redundant filterbank precoders and equalizers. I. Unification and optimal designs, IEEE Trans. Signal Process. 47 (7) (July 1999) 1988–2006.

[31] S. Weiss, R.W. Stewart, Fast implementation of oversampled modulated filter banks, Electronics Lett. 36 (17) (August 2000) 1502–1503.

[32] Y.-J. Chen, S. Oraintara, K. Amaratunga, Dyadic-based factorizations for regular paraunitary filterbanks and m-band orthogonal wavelets with structural vanishing moments, IEEE Trans. Signal Process. 53 (1) (January 2005) 193–207.

[33] Z. Cvetkovic, M. Vetterli, Tight Weyl–Heisenberg frames in $l^2(z)$, IEEE Trans. Signal Process. 46 (5) (May 1998) 1256–1259.

[34] T.M. Apostol, Introduction to Analytic Number Theory, Springer, Berlin, 1976.

[35] Y.-P. Lin, S.-M. Phoong, ISI-free FIR filterbank transceivers for frequency-selective channels, IEEE Trans. Signal Process. 49 (11) (November 2001) 2648–2658.

[36] J. Nocedal, S.J. Wright, Numerical Optimization, second ed., Springer, Berlin, 2006.

[37] R.H. Byrd, P. Lu, J. Nocedal, A limited memory algorithm for bound constrained optimization, SIAM J. Sci. Statist. Comput. 16 (5) (1995) 1190–1208.

[38] C. Zhu, R.H. Byrd, J. Nocedal, L-BFGS-B: Algorithm 778: L-BFGS-B, FORTRAN routines for large scale bound constrained optimization, ACM Trans. Math. Software 23 (4) (1997) 550–560.

[39] M.R. Wilbur, T.N. Davidson, J.P. Reilly, Efficient design of oversampled NPR GDFT filterbanks, IEEE Trans. Signal Process. 52 (7) (July 2004) 1947–1963.

[40] J.G. Proakis, D.G. Manolakis, Digital Signal Processing: Principles, Algorithms, and Applications, third ed., Prentice-Hall, Englewood Cliffs, NJ, 1996.

[41] R.K. Martin, K. Vanbleu, M. Ding, G. Ysebaert, M. Milosevic, B.L. Evans, M. Moonen, C.R. Johnson Jr., Unification and evaluation of equalization structures and design algorithms for discrete multitone modulation systems, IEEE Trans. Signal Process. 53 (10) (October 2005) 3880–3894.

[42] J.A.C. Bingham, RFI suppression in multicarrier transmission systems, in: Proceedings of the Global Telecommunications Conference, vol. 2, November 1996, pp. 1026–1030.

[43] J.M. Cioffi, A multicarrier primer, Amati Communication Corporation and Stanford University, T1E1 contribution T1E1.4/97-157, November 1991.

[44] P. Charbonneau, Genetic algorithms in astronomy and astrophysics, Astrophys. J. Suppl. Ser. 101 (12) (December 1995) 309–334.